Mixed Matrix PVDF Hollow Fiber Membranes with Nanoscale Pores for Desalination through Direct Contact Membrane Distillation

ARTICLE *in* INDUSTRIAL & ENGINEERING CHEMISTRY RESEARCH · APRIL 2009

Impact Factor: 2.59 · DOI: 10.1021/ie8009704

3 AUTHORS, INCLUDING:

Tai-Shung Chung
National University of Singapore
720 PUBLICATIONS **19,017** CITATIONS

SEE PROFILE

Mixed Matrix PVDF Hollow Fiber Membranes with Nanoscale Pores for Desalination through Direct Contact Membrane Distillation

Kai Yu Wang, Suay Wei Foo, and Tai-Shung Chung*

Department of Chemical and Biomolecular Engineering, National University of Singapore, 4 Engineering Drive 4, Singapore 117576

Highly porous hydrophobic hollow fiber membranes with high porosity and sandwich trilayer structure were specially designed to meet the requirements of direct contact membrane distillation (DCMD). Poly(vinylidene fluoride) (PVDF)/Cloisite clay composite hollow fibers were fabricated based on the dry-jet wet phase inversion mechanism by using water as both the external and internal coagulants. Membrane void fraction of up to 90% can be produced to improve the fibers' thermal insulation and reduce vapor transport resistance. The fiber inner surface was full of streaky pores with pore size less than 1.0 μm in diameter, while the pores on the fiber outer surface were much smaller, less than 50 nm in diameter. This demonstrates that membrane pores fabricated at a nanoscale can achieve high water vapor permeation flux with 100% salt rejection. For example, the fabricated PVDF/clay composite hollow fiber was tested by desalinating a 3.5 wt % NaCl solution and permeation flux as high as 79.2 kg/(m^2·h) (calculated on the fiber outer diameter) was achieved at the inlet temperatures of 81.5/17.5 °C. The performance shows almost no decay during 220-h continuous tests. The addition of clay particles may enhance the tensile modulus and improve long-term stability compared to those fibers without particles.

1. Introduction

Membrane distillation (MD), the combination of water evaporation and vapor condensation in an integrated membrane process, has been investigated over the past 40 years. The porous hydrophobic membrane, serving as both a thermal insulation and a physical barrier, permits the free transport of water vapor through the pores but prevents the liquid phase from getting through the membrane due to surface tension forces. As a result, 100% rejection of the nonvolatile solute can theoretically be achieved. Compared to conventional separation processes, MD has advantages in seawater desalination and solution concentration due to its mass and heat transfer mechanisms. MD exhibits the potential to compete with conventional but energetically intensive techniques[1,2] such as distillation, evaporation, and reverse osmosis because MD can be operated under low temperatures or low pressures with high productivity. Moreover, low-grade, waste, and/or alternative natural energy sources such as solar and geothermal energy can be utilized to make MD a low operating cost separation process.

The membrane, which acts as the physical barrier between two phases and provides a liquid−gas interface for heat and mass exchanges but is not involved in the separation, plays a very important role in realizing the MD process. Most commercially available hydrophobic flat sheet or hollow fiber membranes used in MD, such as polypropylene (PP), polyethylene (PE), polytetrafluoroethylene (PTFE), and poly(vinylidene fluoride) (PVDF) membranes,[3] are fabricated by means of melt spinning plus stretching or thermally induced phase separation (TIPS) under high temperatures. Even though these commercially available membranes have low surface energy, i.e., hydrophobic property, and low thermal conductivity, their bulk and surface porosity, and other physicochemical properties, cannot meet the requirements for high performance MD processes because they were originally produced for other applications.

* To whom correspondence should be addressed. Fax: (65) 6779-1936. E-mail: chencts@nus.edu.sg.

In the MD process, the aqueous feed solution to be treated must be in direct contact with one side of the membrane without penetrating through its dry pores. Liquid/vapor interfaces are formed at the entrances of membrane pores, and vapor diffuses through the pores. In order to prevent the fluid from entering the membrane pores, operating pressure must be kept below the breakthrough pressure (or liquid entry pressure, LEP), which can be calculated by using the Laplace−Yang equation:[1,2]

$$\mathrm{LEP} = -\frac{2\Theta\gamma\cos\theta}{r_{\max}} \tag{1}$$

where γ is the interfacial tension, Θ is a geometric factor related to the pore structure (equal to 1 for cylindrical pores), and θ is the liquid−solid contact angle.

Generally, two approaches can be taken to increase the LEP value: by improving the membrane−water contact angle and by reducing the surface pore size.[4] A higher membrane−water contact angle can be obtained by improving the membrane hydrophobic character. This has been done by using a copolymer of PTFE and PVDF,[5] fluorinated coating or modifying the membrane surface.[6−10] However, it is somewhat limiting to only increase the intrinsic contact angle based on material chemistry as water surface tension will decrease along with an increase in temperature. The reduction of membrane pore size can serve as an alternative and more effective means to prevent liquid from passing through the membrane pores. Generally, pore sizes in the range of 0.1−1.0 μm are considered favorable for direct contact membrane distillation.[11] Drioli[12] and Schneider with their co-workers[13] recommended a maximum pore radius of 0.5−0.6 μm. This value ensures that solution temperature, process pressure, and salt concentration fluctuations do not result in membrane wetting. However, reducing pore size may decrease the membrane surface porosity and increase tortuosity, which will produce a lower permeate flux. Therefore, it is necessary to design new membrane structures with the decreased pore size and improved porosity. Higher membrane porosity corresponds to a larger diffusion area inside the membrane

10.1021/ie8009704 CCC: $40.75
Published on Web 03/26/2009

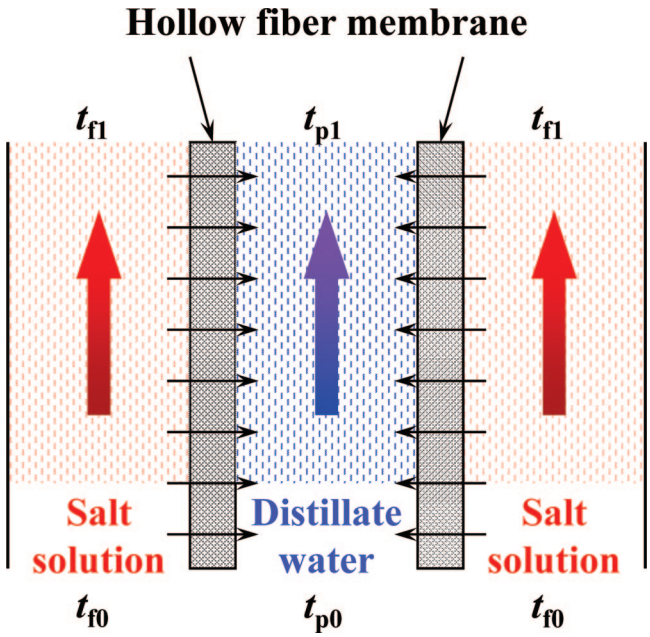

Figure 1. Heat and mass transfer in DCMD.

which lessens vapor transport resistance. In addition, higher porosity also reduces the amount of heat lost by conduction.

PVDF is chosen in this study for membrane preparation because it is a commercially available hydrophobic polymer which can be easily dissolved in many common aprotic solvents used in hollow fiber spinning. PVDF hollow fiber membranes have been fabricated using the nonsolvent induced wet phase inversion process. These membranes are mainly used in ultrafiltration for water treatment,[14,15] and in vacuum membrane distillation (VMD) to remove benzene/toluene[16] or volatile organic compounds (VOCs).[17] Some flat sheet membranes have also been developed for pervaporation and VMD[18] and MD.[19] Dual-layer hydrophobic/hydrophilic PVDF hollow fiber membrane[20] and single-layer hollow fiber[21−23] have been fabricated using the nonsolvent induced wet phase inversion process and are tested by using direct contact membrane distillation (DCMD). The study of the effects of membrane formation on membrane structure and performance in MD is still underway.

Hollow fibers have been widely used for liquid phase separation due to their high surface area to volume ratio and ability to self-support. DCMD is one of the MD configurations whereby the hydrophobic membrane comes into direct contact with two liquid streams (i.e., the hot feed and the cold permeate streams), as shown in Figure 1. The hollow fiber used in DCMD must have low heat conductivity to improve the thermal efficiency, low vapor transfer resistance to enhance the permeate flux, and stable mechanical strength to conduct long time operation. Two kinds of additives were added to modify the PVDF membrane characteristics. One is ethylene glycol (EG) because it has a high boiling point (193.1 °C at 1.0 atm) and a solubility parameter of 32.9 $MPa^{1/2}$ just between those of *N*-methyl-1-pyrrolidone (NMP, solvent 22.9 $MPa^{1/2}$)/PVDF (23.2 $MPa^{1/2}$) and water (coagulant, 47.8 $MPa^{1/2}$). Moreover, EG is miscible with water and NMP in all proportions and can easily be removed from the membrane after spinning. EG has been used as the additive to enhance pore formation during phase inversion.[14,21,24] The other additive is clay particles as they can reinforce fiber mechanical strength and control the coefficients of thermal expansion and heat insulation by forming a kind of mixed matrix membrane embedded with a dispersed inorganic phase.[25−27]

Therefore, the main objective of this work is to develop a novel type of mixed matrix hydrophobic hollow fiber membrane with nanosized pores to enhance desalination in DCMD. The effect of additives on the membrane structure and performance will be investigated.

2. Experimental Section

2.1. Materials. Kureha PVDF1300 resin (specific gravity 1.77, T_g −38 °C) was supplied by Kureha Corp., Japan. The organophilic clay, Cloisite 20A, a natural montmorillonite modified with a dimethyl, dihydrogenated tallow quaternary ammonium salt, was purchased from Southern Clay (Gonzales, TX). NMP (>99.5%), was used as solvent and ethylene glycol (EG, >99.5%) was used as a nonsolvent in the polymer solution. Sodium chloride (NaCl, 99.5%) was purchased from Merck, Germany. The ultrapure water used in all experiments was produced by a Milli-Q unit (MilliPore, USA) with the resistivity of 18 MΩ cm.

2.2. Preparation of PVDF Polymer Solution. The spinning dope of PVDF/NMP/Cloisite 20A/EG was prepared by dissolving the PVDF and clay powder in the NMP and EG mixture, while stirring, until the solution became uniform. The addition of EG as a nonsolvent has two functions: not only can it result in rapid phase separation, thus obtaining a thin skin layer, it also behaves as a pore-forming agent to produce membranes with a porous structure. Another PVDF/NMP/EG dope was prepared as comparison by dissolving the dried PVDF powder in the NMP/EG mixture.

2.3. Fabrication of PVDF Hollow Fiber Membranes. The hollow fiber spinning process through the dry-jet wet phase inversion is schematically described elsewhere.[21] The formulated uniform polymer solutions were degassed before spinning. The pulse-free bore fluid and dopes were fed into the inner tube and the annulus of the spinneret separately through flow meters by two ISCO syringe pumps. Tables 1 and 2 list the detailed hollow fiber spinning parameters. In the two batches of hollow fiber spinning, the concentrations of PVDF polymer and the additive of EG in the dopes were prepared at the same concentration and the dope flow rates kept constant. Tap water was used as both the internal and external coagulants to solidify the PVDF polymer solution and form hollow fiber membranes. The as-spun fibers were immersed in water for 3−5 days to remove the residual NMP and EG. The wet fibers were then frozen in a freezer for about 2 h and vacuum-dried using a freeze-dryer (S61-Modulyo-D, Thermo Electron Corp., USA) for about 12 h. To ensure reproducibility, hollow fibers were spun under the same conditions at least two times. The purpose of using a freeze-dryer is to avoid pore closing for hydrophobic PVDF hollow fibers.

2.4. Morphology Study. The freeze-dried hollow fiber samples were immersed in liquid nitrogen and fractured, and then sputtered with platinum using a JEOL JFC-1100E ion sputtering device. The cross section, inner layer, and outer layer of samples were observed under field emission scanning electron microscopy (FESEM; JEOL JSM-6700).

The void fraction, ε, of the PVDF hollow fiber was calculated by

$$\varepsilon = \left(1 - \frac{\rho_{\text{fiber}}}{\rho_{\text{PVDF}}}\right) \times 100\% \qquad (2)$$

where ρ_{fiber} and ρ_{PVDF} are the densities of the fiber and the PVDF material, respectively.

Table 1. Spinning Conditions of Fabricating PVDF Hollow Fiber Membranes

hollow fiber sample[a]	Kureha-A	Kureha-B	Kureha-C
dope solution composition (wt %)		PVDF/NMP/EG (10.0/78.0/12.0)	
dope flow rate (mL min^{-1})	4.0	4.0	4.0
bore fluid composition		tap water	
bore fluid flow rate (mL min^{-1})	2.66	4.0	5.3
external coagulant		tap water	
air gap distance (cm)		2.0	
hollow fiber dimension o.d./i.d. (μm)	1200/760	1290/920	1340/1020
fiber wall thickness (μm)	220	185	160
contact angle (deg)	82.9 ± 0.8	81.5 ± 1.0	80.0 ± 1.0
hollow fiber porosity, ε (%)	91.7 ± 0.6	90.1 ± 0.4	89.6 ± 0.4
membrane thermal conductivity,[b] k_m (W m^{-1} K^{-1})	0.042 ± 0.001	0.043 ± 0.001	0.044 ± 0.001

[a] All the hollow fibers were fabricated under free drawing spinning. [b] Calculated according to eq 4 at 75 °C.

Table 2. Spinning Conditions of Fabricating PVDF/Clay Composite Hollow Fiber Membranes

hollow fiber sample[a]	Kureha20A-A	Kureha20A-B	Kureha20A-C
dope solution composition (wt %)		PVDF/NMP/Cloisite 20A/EG (10.0/74.7/3.3/12.0)	
dope flow rate (mL min^{-1})	4.0	4.0	4.0
bore fluid composition		tap water	
bore fluid flow rate (mL min^{-1})	2.66	4.0	5.3
external coagulant		tap water	
air gap distance (cm)		2.0	
hollow fiber dimension o.d./i.d. (μm)	1300/800	1360/960	1380/1020
fiber wall thickness (μm)	250	200	180
contact angle (deg)	86.8 ± 1.0	87.1 ± 0.8	86.2 ± 1.0
hollow fiber void fraction, ε (%)	88.9 ± 0.7	87.6 ± 0.5	86.7 ± 0.4
membrane thermal conductivity,[b] k_m (W m^{-1} K^{-1})	0.047 ± 0.001	0.049 ± 0.001	0.050 ± 0.001

[a] All the hollow fibers were fabricated under free drawing spinning. [b] Calculated according to eq 4 at 75 °C.

2.5. Contact Angle Measurement. The dynamic contact angle θ of the PVDF hollow fiber at 25 °C was measured with a KSV Sigma 701 tensiometer (KSV Instruments Ltd., Finland). The tensiometric method determines the advancing contact angle by measuring the force when a sample of fiber is brought into vertical contact with deionized water. As the forces of interaction and geometry of the solid were measured with a known surface tension of water, the dynamic contact angle can be calculated. The advantages of this method are that the actual measurement is simple to perform and the wetting characteristics of a single fiber can easily be obtained.

2.6. Mechanical Property Test. Tensile strength tests was conducted on the as-spun hollow fiber membranes using an Instron tensiometer (Model 5542, Instron Corp., USA) at room temperature. The fiber sample was clamped at both ends and pulled in tension at a constant elongation rate of 50 mm min^{-1} with an initial gauge length of 25 cm. Tensile stress at break, tensile strain, and Young's modulus were obtained from the stress−strain curves as the average of at least 10 measurements.

2.7. Performance of PVDF Hollow Fiber in DCMD. The dry PVDF hollow fibers with a length of 20 cm were assembled in a plastic tube (diameter 3/8 in.) to form a membrane module. Each membrane module had a filtration area of 100 ± 5 cm^2. The packing fraction of hollow fiber in the module was around 30−40%. Three hollow fiber modules from the same spinning condition were fabricated for testing, and their performance average was used for comparison. DCMD experiments were conducted on a laboratory-scale circulating unit, as shown in Figure 2. The membrane module was vertically mounted on the MD installation to eliminate the effect of free convection and to remove air bubbles contained in the streams. Because the outer surface of hollow fibers facing the shell side was the selective layer, the hot salt solution flowed through the shell side, whereas the cold distillate water flowed through the lumen side. The hot salt solution and cold distillate water flowed cocurrently through the module from the bottom to the top, to induce similar pressures on opposite sides of the membrane at all points, thus decreasing the risk of membrane wetting. The pressure on the distillate side was kept 0.5 psi higher than that on the hot salt solution side to prevent salt leakage. The temperatures and pressures of two streams were monitored at the inlets and outlets of the hollow fiber module by thermocouples and pressure gauges. The hollow fiber module was insulated with thermal insulation tapes.

Solution temperatures were controlled by two water baths and measured with thermocouples with an accuracy of ±0.1 °C. The inlet temperature of cold distillate water was kept constant at 17.5 °C. The inlet temperature of the hot solution was varied in the range 40−85 °C. The NaCl concentration in the hot salt solution was kept constant at 3.5 wt % except for special cases. The NaCl concentration in the cold distillate water was measured with an electric conductivity meter (Pioneer30, Radiometer, Neuilly-Plaisance, France). The weight gain on the distillate side at each feed temperature was measured over a predetermined period after the outlet temperatures reached steady state. The permeation flux, J_v (kg m^{-2} h^{-1}), was calculated from the equation

$$J_v = \frac{\Delta W}{A \Delta t} \tag{3}$$

where ΔW (kg) is the permeation weight collected over a predetermined time Δt (h) of DCMD process duration; A (m^2) is the effective permeation area (based on the external diameter of hollow fibers).

3. Results and Discussion

3.1. Morphology Studies of Composite Hollow Fiber Membranes. Figure 3 illustrates the sandwich structure of the PVDF hollow fibers. The sandwich structure consists of three layers, where a thin, spongelike porous layer is located between two thick layers full of fingerlike macrovoids. Larger fingerlike macrovoids and the spongelike pore network contain a large volume of air which can increase the membrane void fraction. The membrane void fraction reaches 88.9% and 91.7% for fibers with and without clay particles, respectively. This kind of

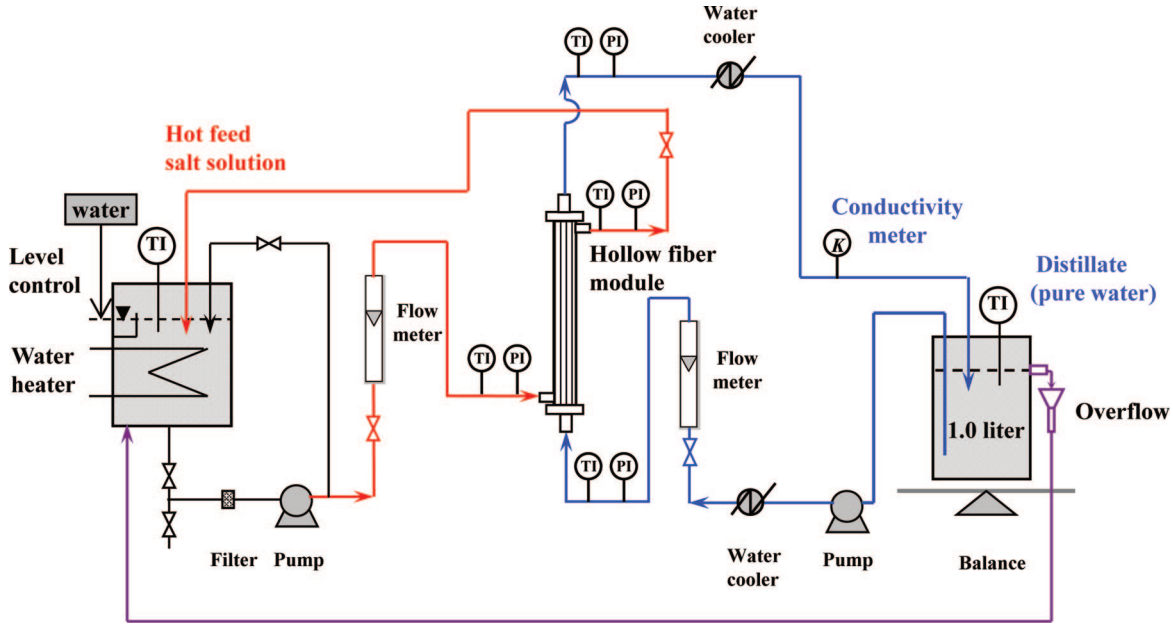

Figure 2. Schematic of the laboratory-scale direct contact membrane distillation setup.

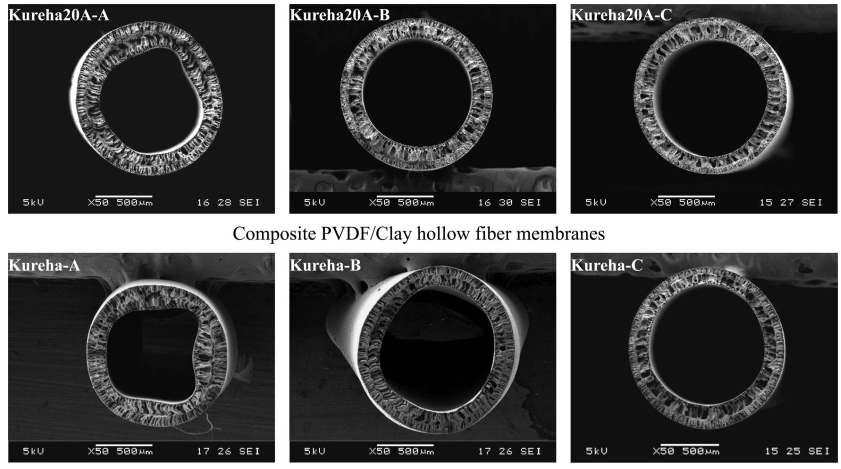

Figure 3. SEM morphology of PVDF hollow fiber membranes.

microstructure provides PVDF hollow fiber with less resistance for water vapor transport through the membrane. There is a slight difference among the fibers spun from different spinning conditions. A higher bore fluid rate during spinning leads to a lower membrane void fraction which may be attributed to the bore fluid's squashing on the nascent fiber.

The higher membrane void fraction results in lower heat conduction between the two streams during DCMD. The membrane thermal conductivity k_m is generally used to evaluate the membrane conductivity and is given by[28]

$$k_m = \varepsilon k_g + (1 - \varepsilon)k_s \tag{4}$$

where ε is the membrane void fraction, and k_s and k_g are the thermal conductivities of the solid membrane material and of the vapor/air within the pores, respectively. The thermal conductivity of the PVDF material and the air at 323 K were taken by interpolating from the reported data in literature as follows: 0.19 W m^{-1} K^{-1} for PVDF and 0.028 W m^{-1} K^{-1} for air/vapor.[29] The calculated k_m values are in the range 0.04−0.05 W m^{-1} K^{-1} (75 °C) given in Tables 1 and 2.

In both batches of hollow fibers, the fiber wall thickness is in the range 150−250 μm. It was found that when the fibers were spun at a low bore fluid flow rate, the fiber inner contour deformed (i.e., noncircular), such that the fiber wall thickness is no longer uniform.[30] Because water is used as the internal coagulant during fiber spinning, phase inversion takes place in the inner dope layer immediately after the polymer solution extrudes from the spinneret and meets with the bore fluid (water) at the spinneret outlet. During this period, the external dope layer is still in contact with air and is thus still in the liquid phase. This remains until the external dope layer meets with the external coagulant (water). Then, when the phase inversion takes place on the outer layer of nascent fiber, the inward radial forces generated by the shrinkage of nascent fiber outer layer will buckle the rigid elastic shell formed in the interface between the bore fluid and the dope solution.[31] As a result, the elastic and buckling instability will provoke the development of a nonuniform cross section of hollow fibers. When the bore fluid flow rate is increased, the deformed inner contour disappears but the fiber external diameter increases and the fiber wall thickness decreases. The increase in the bore fluid flow rate will

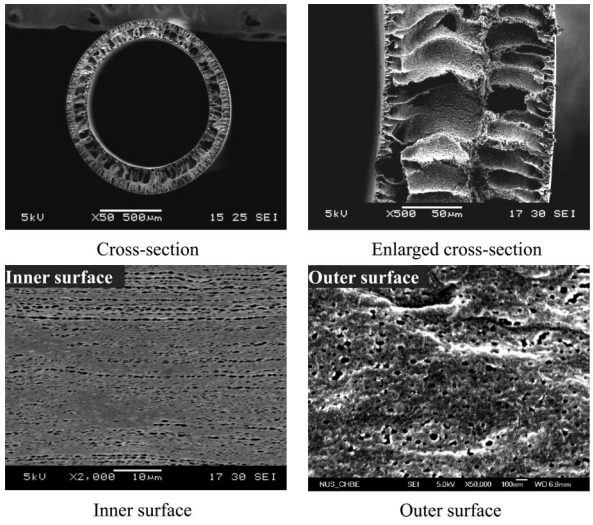

Figure 4. SEM morphology of composite PVDF hollow fiber membrane (Kureha20A-C).

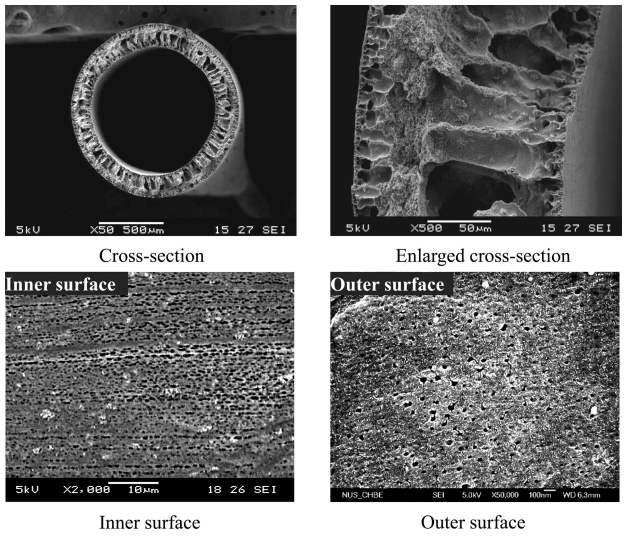

Figure 5. SEM morphology of PVDF hollow fiber membrane (Kureha-C).

balance the inward radial forces induced by the solidification of outer layer dope and maintain a circular fiber inner contour.

On the fiber outer surface, as shown in Figures 4 and 5, the circular pores with pore size less than 50 nm in diameter are quite different from those pores made by a melt-spinning process plus stretching. The pore size of such a scale is much smaller than those commercially available Celgard[19,20] and Accurel PP membranes,[32] Gore PTFE,[29] and Millipore PVDF[33] membranes. On the inner surface, the streaky pores develop in parallel along the axial direction, i.e., the spinning line direction. The streaking of pores on the inner surface developed along the direction of bore fluid flowing is attributed to the shear stress on the polymer solution induced within the spinneret. After the polymer solution is extruded from the spinneret outlet, the phase inversion takes place when meeting the strong coagulant of water immediately and the oriented polymer chains have no time to relax. As a result, the formed pores are elongated along the spinning line. The inner surface pore size is less than 1.0 μm in diameter, and it is much larger than that on the fiber outer surface. Therefore, water cannot penetrate pores on either side of the hydrophobic membranes during DCMD under low pressures.

From Figure 6, it can be found that the clay particles are embedded in the polymer matrix and concentrated in the middle spongelike area. This is because the middle of the cross section experienced low shear stresses.[34,35] The hydrophobic clay particles not only act as the bridging point to enhance the fiber mechanical strength, but also increase tortuosity and hydrophobicity without significantly changing the overall membrane porosity. This can be verified by the increased contact angles of PVDF/clay composite membranes compared to fibers without clay particles, as listed in Tables 1 and 2.

3.2. Water Transport during DCMD. During DCMD, two streams, a cold fresh water distillate and a 3.5 wt % NaCl hot aqueous solution, flow through the lumen and shell sides of hollow fibers, respectively. The water permeation flux based on the fiber external surface area is shown in Figures 7 and 8. Water vapor flux of 79.2 kg/(m^2·h) (Kureha20A-C) can be achieved at the inlet temperatures of 81.5/17.5 °C, respectively. For fibers without clay particles, the permeation flux reaches even higher. In addition, increasing the bore fluid flow rate during spinning improves the water permeation flux at the same temperature. This may be due to the decrease in fiber wall thickness which reduces the vapor transport resistance.

Compared with commercial membranes used in DCMD, the synthesized PVDF fibers exhibit higher water permeation flux. This enhanced performance is due to the improved membrane porosity induced by the addition of ethylene glycol (EG) and novel cross-section morphology. As for the permeate quality, the solution conductivity in the cold distillate water is less than 5.0 μs cm^{-1} during the DCMD operation, indicating that 100% NaCl rejection is achieved.

The water vapor transport inside the porous membrane under isothermal conditions can be described by three major mechanisms based on the dusty gas model:[36] Knudsen diffusion, viscous flow, and molecular diffusion. The combinations of these transport models such as Knudsen−viscous transition and Knudsen−molecular diffusion transition can establish the mass transfer mechanism during membrane distillation.[33] The Knudsen number (Kn) is used to classify the regions, and is defined as the ratio of the mean molecular free path of the gas to the pore diameter:

$$Kn = \lambda/d_p \tag{5}$$

For the binary mixture of water vapor and air, the mean molecular free path of water in air (λ_{w-a}) is evaluated at the average membrane temperature (T_m):[37]

$$\lambda_{w-a} = \frac{k_B T_m}{\pi\left(\frac{\sigma_w + \sigma_a}{2}\right)^2 P_T} \frac{1}{\sqrt{1 + (M_w/M_a)}} \tag{6}$$

where k_B is the Boltzmann constant (1.381 × 10^{-23} J K^{-1}), P_T is the absolute pressure (Pa), σ_w and σ_a are the collision diameters for water vapor (2.641 × 10^{-10} m) and air (3.711 × 10^{-10} m),[38] and M_w and M_a are the molecular weights of water and air. At the typical membrane temperature of 60 °C and pressure of 1.013 × 10^5 Pa in DCMD, the mean free path of water in air is 0.182 μm larger than the pore diameter (maximum of 50 nm on the outer surface) on the membrane surface for both batches of hollow fibers. Therefore, the combination of Knudsen diffusion and molecular diffusion of vapor transport through the membrane pores is responsible for mass transport in DCMD.[33,39]

3.3. Effect of Flow Rates on the Water Permeation Flux. Figures 9 and 10 show that the flux increases slightly when the recirculation rate of hot NaCl solution is increased. This is due to the fact that a higher recirculation rate can increase

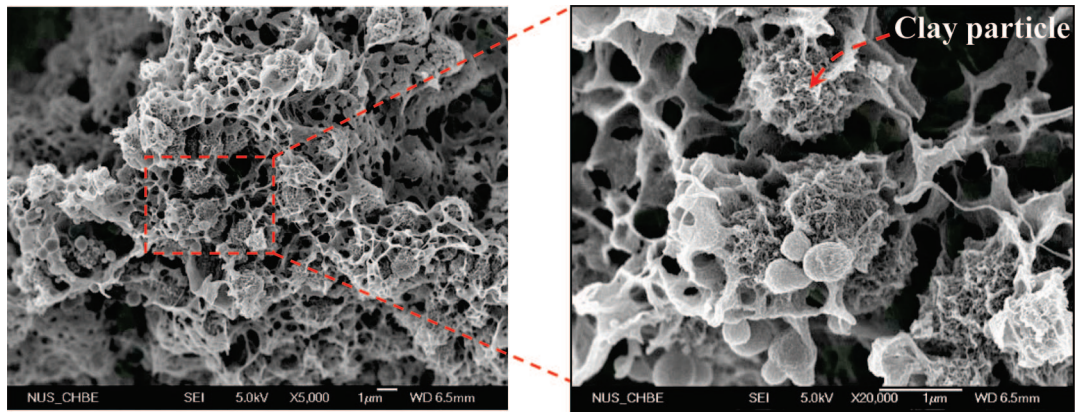

Figure 6. Distribution of clay particles in the polymer matrix (Kureha20A-C).

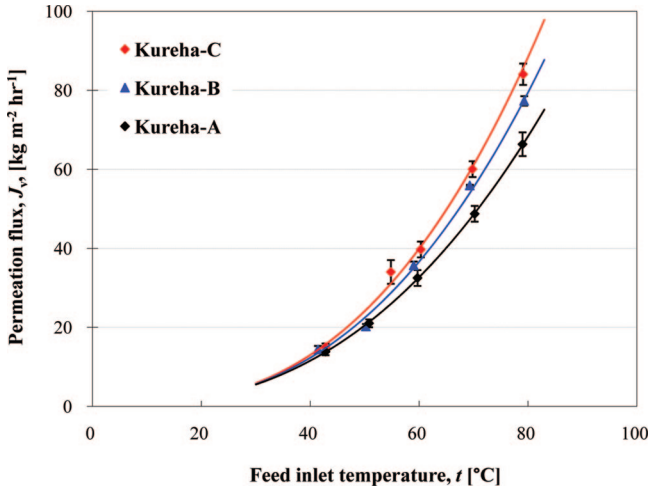

Figure 7. Permeation flux vs hot salt solution inlet temperature t_f. Salt solution: flow rate 1.8 m s^{-1}. Cold distillate water: 17.5 °C, flow rate 1.2 m s^{-1}.

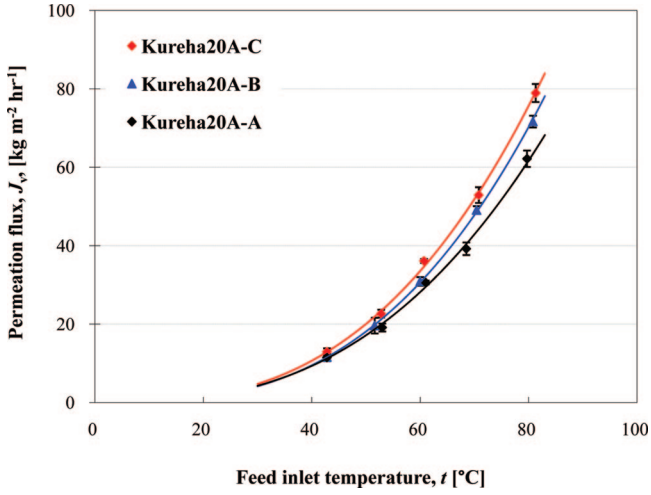

Figure 8. Permeation flux vs hot salt solution inlet temperature t_f. Salt solution: flow rate 1.8 m s^{-1}. Cold distillate water: 17.5 °C, flow rate 1.2 m s^{-1}.

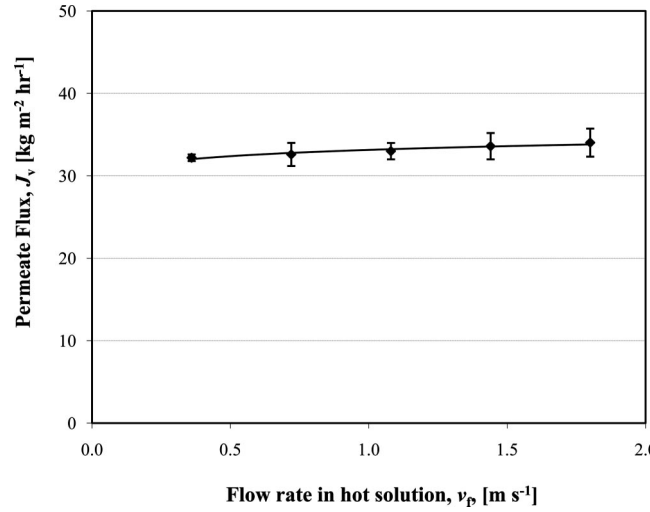

Figure 9. Permeation flux vs flow rate of hot salt solution, v_f (Kureha20A-C). Salt solution: 60.3 °C. Cold distillate water: 17.5 °C, 1.2 m s^{-1}.

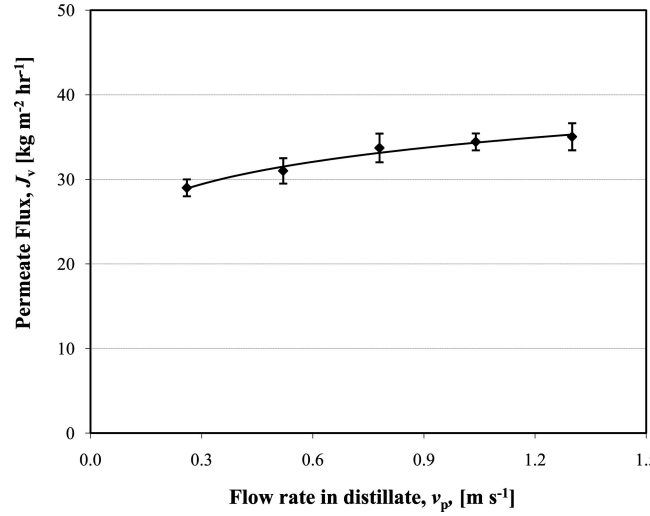

Figure 10. Permeation flux vs distillate flow rate, v_p (Kureha20A-C). Salt solution: 60.3 °C, 1.8 m s^{-1}. Cold distillate water: 17.5 °C.

the heat transfer coefficient and thus reduce the effect of temperature polarization and concentration polarization. In addition, the membrane surface temperatures will be brought closer to that of the bulk streams, and the transmembrane temperature difference is thus increased. This produces a larger driving force and consequently enhances the flux. However, the heat loss by conduction across the membrane is also enhanced.

Comparing Figures 9 and 10 with Figure 7, the effect of recirculation rates on water flux seem to be less than that of the feed temperature differences.

3.4. Effect of Salt Concentration on the Membrane Performance. Figure 11 demonstrates the water flux versus the concentration of NaCl feed solutions under 60 °C. Compared

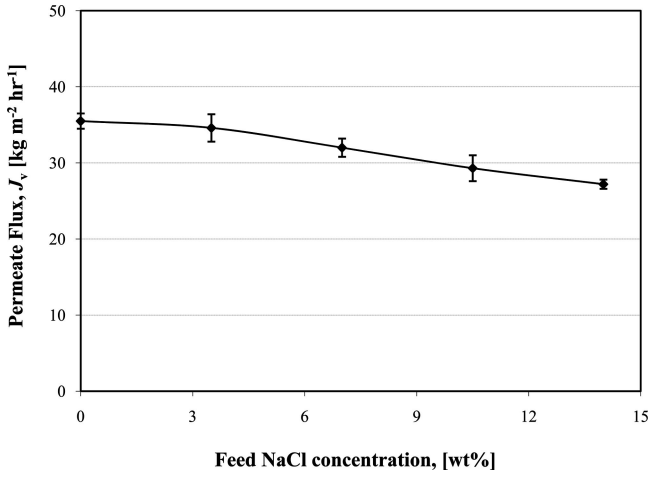

Figure 11. Permeation flux vs NaCl concentration in the hot salt solution (Kureha20A-C).

with the flux when pure water is used as the feed solution, there is a 21.5% decrease in flux when a 14 wt % NaCl feed solution is treated while the quality of the permeate water is only marginally affected. The reduction of water vapor pressure under high solute concentrations is the main reason for the decrease in permeation flux under the same temperature. This is due to the decrease in the water activity and concentration. Other reasons may include the concentration and thermal polarization in the boundary layer of the hot feed solution which leads to decreases in heat and mass transfer coefficients in the boundary layer. This results in the increase in NaCl concentration on the membrane surface and the decrease in membrane surface temperature.[40]

3.5. Long Time Performance during Desalination. During the long time testing of the membrane performance of the fabricated PVDF fibers, water permeate condensed in the distillate side is returned to the feed tank in order to maintain the salt concentration of the hot stream, as shown in Figure 2. The Kureha20A-C composite hollow fiber is selected to conduct the long time continuous testing over a period of 220 h. From the result as shown in Figure 12, it can be seen that the water flux declines by 10% in the first 20 h, and then levels off with the quality of the permeate water only slightly affected. The composite PVDF hollow fibers containing particles can withstand long time operation and keep a stable vapor permeation flux because of its unique membrane structures. The two fingerlike macrovoid layers greatly decrease the vapor transport resistance and act as a thermal insulator barrier to reduce heat conduction, while the thin middle spongelike layer unites two macrovoid layers to make the whole membrane become an integrated structure at the aid of clay particles. Although a high permeation flux can be produced for PVDF hollow fiber without particles, these membranes cannot maintain long time running due to fiber collapse and other issues. The membrane ductile capacity (extension at break), stretch resistance (tensile at break), and rigidity (in the form of Young's modulus) are listed in Table 3. By comparing with the PVDF hollow fibers, the tensile strength and the strain at break of the PVDF/clay composite hollow fibers decrease with the addition of clay. However, the Young's modulus is increased for the PVDF/clay composite fibers compared with neat PVDF fibers.

3.6. Thermal Efficiency of DCMD. Heat transfer during MD consists mainly of two parts: the latent heat transfer due to the water vaporization and condensation and the heat conduction across the membrane. The thermal conduction from the hot stream to the cold stream, together with the latent heat of water evaporation, contributed to temperature decrease from the inlet of the shell side to the outlet and vice versa for the lumen side. Thermal efficiency, EE, is defined as the ratio between the heat which contributes to evaporation and the total heat exchanged between two streams.[41] Because distillate water flows through the fiber lumen side, there is no other heat transfer except for heat from the fiber shell side. For simplification, the total heat exchange can be calculated from the enthalpy difference between the inlet and outlet of the distillate water

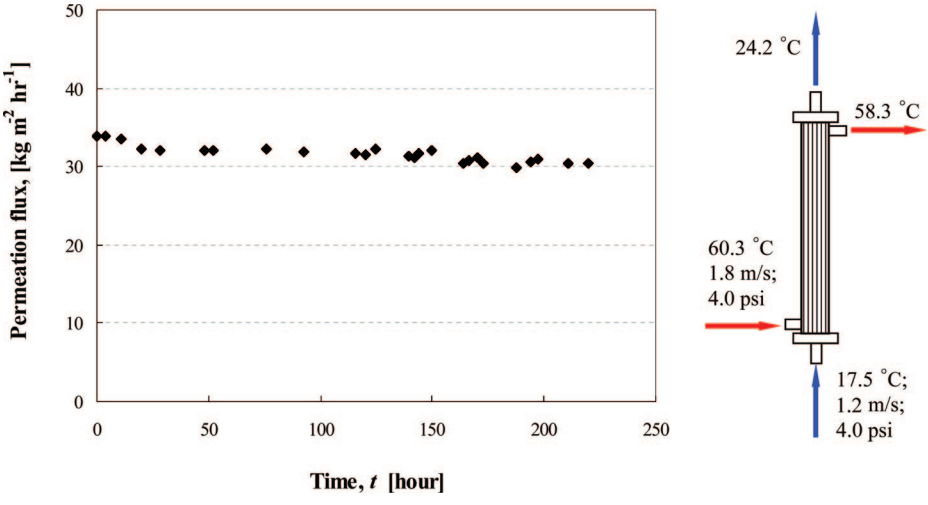

Figure 12. Variation of water vapor flux along with operating time (Kureha20A-C). Hot brine: 3.5 wt % NaCl, 60.3 °C, 1.8 m s^{-1}. Cold distillate water: 17.5 °C, 1.2 m s^{-1}.

Table 3. Mechanical Properties of PVDF and PVDF/Clay Composite Hollow Fiber Membranes

hollow fiber sample	Kureha-A	Kureha-B	Kureha-C	Kureha20A-A	Kureha20A-B	Kureha20A-C
strain at break (%)	171 ± 5	177 ± 7	185 ± 4	103 ± 6	109 ± 4	115 ± 7
tensile stress at break (MPa)	1.13 ± 0.06	1.21 ± 0.07	1.28 ± 0.06	0.73 ± 0.04	0.88 ± 0.05	0.95 ± 0.06
Young's modulus (MPa)	15.6 ± 1.5	17.9 ± 2.4	19.8 ± 1.7	18.6 ± 1.6	22.4 ± 2.4	26.1 ± 1.9

Table 4. Comparison of PVDF Membranes for DCMD

membrane	manufacturer	hot feed solution: NaCl concentration	hot feed solution: t_1 (°C)	hot feed solution: flow rate (m s^{-1})	cold distillate: t_2 (°C)	cold distillate: flow rate (m s^{-1})	permeation flux[a] (kg m^{-2} h^{-1})	ref
GVHP PVDF flat sheet, thickness 126 μm	Millipore	distilled water	70	2.59	20	4.67	32.4	33
PVDF/PAN dual-layer hollow fiber, i.d. 520 μm, thickness 340 μm	laboratory scale	3.5 wt %	90	1.60	16.5	0.80	55	10
PVDF composite hollow fiber, i.d. 600 μm, thickness 110 μm	laboratory scale	3.5 wt %	79.3	1.60	17.5	0.80	41.5 ± 1.4	11
PVDF hollow fiber, i.d. 680 μm, thickness 140 μm	laboratory scale	3.5 wt %	79.5	1.9	17.5	0.9	50.4 ± 2.2	12
PVDF composite hollow fiber, i.d. 860 μm, thickness 120 μm.	laboratory scale	3.5 wt %	86.0	1.40	20.5	1.40	70.1	13
PVDF composite hollow fiber, i.d. 1000 μm, thickness 190 μm	laboratory scale	3.5 wt %	81.3	1.8	17.5	1.2	79.2 ± 1.2	this work[b]

[a] The permeation flux of hollow fiber membrane is based on the fiber external diameter. [b] Kureha20A-C.

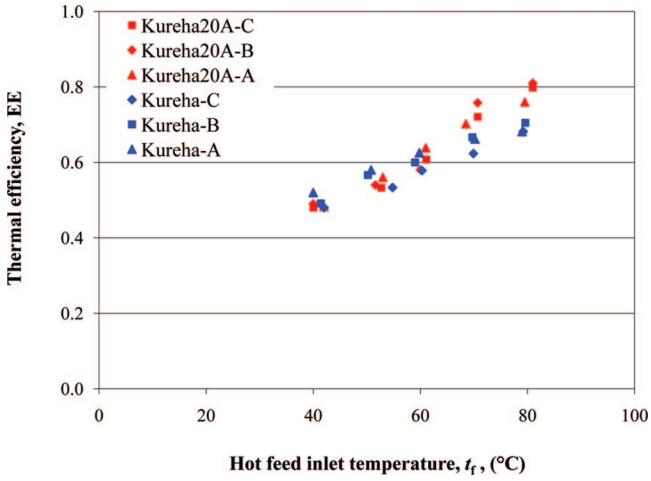

Figure 13. Thermal efficiency vs inlet temperature of hot salt solution, t_f. Hot brine: 3.5 wt % NaCl, 1.8 m s^{-1}. Cold distillate water: 17.5 °C, 1.2 m s^{-1}. Salt solution: 60.3 °C, 1.8 m s^{-1}; cold distillate water: 17.5 °C, 1.2 m s^{-1}.

approximately. For the well-insulated module, EE can be calculated as[9]

$$\mathrm{EE} = \frac{J_v A \Delta H_v}{J_v \Delta H_v + h_m(t_{fm} - t_{pm})} = \frac{J_v A \Delta H_v}{V_p \overline{C_p}(t_{p1} - t_{p0})} \quad (7)$$

where J_v is the vapor permeation flux, ΔH_v is the latent heat of vaporization, h_m is the heat transfer coefficient of membrane, t_{fm} and t_{pm} are the surface temperatures on the two sides of the membrane, V_p is the distillate water flow rate, $\overline{C_p}$ is the average specific heat of water, and t_{p1} and t_{p0} are the temperatures at the outlet and inlet of distillate water.

As shown in Figure 13, the calculated thermal efficiency, EE, varies from 45% to 78% and increases along with the increase in the feed temperature because the vapor permeation flux is exponentially related to temperature. At higher temperatures and the induced high vapor permeation flux, the latent heat of water evaporation is the main contribution to total heat transfer while heat loss due to heat conduction across the membrane is the major contribution to total heat transfer during DCMD at lower temperatures (less than 40 °C). Therefore, the use of high feed temperatures together with membrane materials with low heat conductivity is more thermally efficient for DCMD.

3.7. Comparison with Other PVDF Membranes in DCMD. Table 4 illustrates a comparison of PVDF hydrophobic membranes in the DCMD desalination process between the present work and literature data. It shows that the newly developed laboratory-fabricated PVDF and PVDF/clay composite hollow fibers have higher performance compared to those in published reports. Fabricating PVDF hollow fiber membranes by the nonsolvent induced wet phase inversion process under low temperatures may provide us with an alternative means to tailor membrane dimension and structure for MD applications. Future work will further investigate the effects of membrane scaling as well as temperature and concentration polarization on heat and mass transfer during membrane distillation.

4. Conclusions

In this study, the composite mixed matrix PVDF hollow fiber membranes designed for MD are fabricated through the nonsolvent induced phase inversion and the following remarks can be concluded:

1. The synthesized nanoscale pores on the surface make the membrane quite different from most present membranes with microscale pores used in membrane distillation. This unique property contributes to the 100% salt rejection without the sacrifice of permeation flux.

2. The addition of ethylene glycol in the polymer solution plays a vital role in enhancing pore formation. High porosity is produced but with small pore size on the surface. As a result, high vapor permeation flux through the membrane is achieved.

3. Water can be adopted as both the internal and external coagulants during hollow fiber spinning, providing an alternative approach in fabricating membranes applicable for MD by adjusting the dope components; from an economic and environmental standpoint, the use of water as the coagulant instead of organic solvents may have potential application in industry.

4. The sandwich morphology that consists of a thin spongelike layer located between two fingerlike macrovoid layers makes it possible for membranes to have both low thermal conduction and high vapor permeation flux.

5. The addition of hydrophobic clay particles improves the membrane mechanical stability for long-term tests, although it also results in a slight reduction in water flux compared to fibers without clay particles.

Acknowledgment

The authors thank the A*star and National University of Singapore (NUS) for funding this project with Grants R-279-000-218-305 and R-279-000-218-731. We are appreciative for the supply of Kureha PVDF resin by Kureha Corp., Japan.

Special thanks are due to Mr. Sina Bonyadi and Dr. May May Teoh for their valuable suggestions.

Nomenclature

A = effective permeation area (based on the external diameter of hollow fibers), m^2
$\bar{C}_p$ = average specific heat of water, kJ kg^{-1} K^{-1}
EE = thermal efficiency
J_v = water permeation flux, kg m^{-2} h^{-1}
k_B = Boltzmann constant, 1.381×10^{-23} J K^{-1}
k_g = thermal conductivity of the vapor/air within pores, W m^{-1} K^{-1}
k_s = thermal conductivity of solid membrane material, W m^{-1} K^{-1}
Kn = Knudsen number
h_m = heat transfer coefficient of membrane, W m^{-2} K^{-1}
ΔH_v = latent heat of water vaporization, kJ kg^{-1}
LEP = liquid entry pressure, Pa
M = molecular weights of water and air, g mol^{-1}
P_T = absolute pressure, Pa
Δt = MD process duration, h
t_{fm} = membrane surface temperature on the feed side, °C
t_{pm} = membrane surface temperatures on the distillate side, °C
v = flow rate, m s^{-1}
V_p = distillate water flow rate, kg h^{-1}
ΔW = permeation weight, kg

Greek Symbols

γ = interfacial tension, N m^{-1}
ε = membrane void fraction
ρ = density of the fiber or PVDF material
σ_w = collision diameter for water vapor, m
σ_a = collision diameter for air, m
θ = liquid−solid contact angle, deg
Θ = geometric factor related to the pore structure (=1 for cylindrical pores)

Subscripts

f = feed
g = vapor or air
m = membrane
p = permeate distillate
s = solid membrane material
w = water

Literature Cited

(1) Curcio, E.; Drioli, E. Membrane distillation and related operations—a review. *Sep. Purif. Rev.* **2005**, *34*, 35.

(2) Lawson, K. W.; Lloyd, D. R. Membrane distillation (Review). *J. Membr. Sci.* **1997**, *124*, 1.

(3) Burgoyne, A.; Vahdati, M. M. Review. Direct contact membrane distillation. *Sep. Sci. Technol.* **2000**, *35* (8), 1257.

(4) Gryta, M. Influence of polypropylene membrane surface porosity on the performance of membrane distillation process. *J. Membr. Sci.* **2007**, *287*, 67.

(5) Feng, C.; Shi, B.; Li, G.; Wu, Y. Preliminary research on microporous Membranes F2.4 for membrane distillation. *Sep. Purif. Technol.* **2004**, *39*, 221.

(6) Favia, P.; D'Agostino, R. Plasma treatments and plasma deposition of polymers for biomedical applications. *Surf. Coat. Technol.* **1998**, *98*, 1102.

(7) Khayet, M.; Matsuura, T. Application of surface modifying macromolecules for the preparation of membranes for membrane distillation. *Desalination* **2003**, *158*, 51.

(8) Khayet, M.; Feng, C. Y.; Matsuura, T. Morphological study of fluorinated asymmetric polyetherimide ultrafiltration membranes by surface modifying macromolecules. *J. Membr. Sci.* **2003**, *213*, 159.

(9) Li, B.; Sirkar, K. K. Novel membrane and device for direct contact membrane distillation-based desalination process. *Ind. Eng. Chem. Res.* **2004**, *43*, 5300.

(10) Song, L.; Li, B.; Sirkar, K. K.; Gilron, J. L. Direct contact membrane distillation-based desalination: novel membranes, devices, larger-scale studies, and a model. *Ind. Eng. Chem. Res.* **2007**, *46*, 2307.

(11) El-Bourawi, M. S.; Ding, Z.; Ma, R.; Khayet, M. A framework for better understanding membrane distillation separation process. *J. Membr. Sci.* **2006**, *285*, 4.

(12) Drioli, E.; Wu, Y.; Calabro, V. Membrane distillation in the treatment of aqueous solutions. *J. Membr. Sci.* **1987**, *33*, 277.

(13) Schneider, K.; Holz, W.; Wollbeck, R. Membranes and modules for transmembrane distillation. *J. Membr. Sci.* **1988**, *39*, 25.

(14) Wang, D.; Li, K.; Teo, W. K. Porous PVDF Asymmetric hollow fiber membranes prepared with the use of small molecular additives. *J. Membr. Sci.* **2000**, *178*, 13.

(15) Khayet, M.; Matsuura, T. Preparation and characterization of polyvinylidene fluoride hollow fiber membranes for ultrafiltration. *Polymer* **2002**, *43*, 3879.

(16) Wu, B.; Tan, X.; Teo, W.; Li, K. Removal of benzene/toluene from water by vacuum membrane distillation in a PVDF hollow fiber membrane module. *Sep. Sci. Technol.* **2005**, *40*, 2679.

(17) Khayet, M.; Matsuura, T. Pervaporation and vacuum membrane distillation processes: Modeling and experiments. *AIChE J.* **2004**, *50* (8), 1697.

(18) Gugliuzza, A.; Drioli, E. PVDF and HYFLON AD membranes: Ideal interfaces for contactor applications. *J. Membr. Sci.* **2007**, *300*, 51.

(19) Tomaszewska, M. Preparation and properties of flat-sheet membranes from poly(vinylidene fluoride) for membrane distillation. *Desalination* **1996**, *104*, 1.

(20) Bonyadi, S.; Chung, T. S. Flux enhancement in membrane distillation by fabrication of dual layer hydrophilic-hydrophobic hollow fiber membranes. *J. Membr. Sci.* **2007**, *306*, 134.

(21) Wang, K. Y.; Chung, T. S.; Gryta, M. Fabrication of Hydrophobic PVDF Hollow Fiber Membranes with Narrow pore size distribution and Ultra-thin Skin for the Fresh Water Production through Membrane Distillation. *Chem. Eng. Sci.* **2008**, *63*, 2587.

(22) Bonyadi, S.; Chung, T. S.; Rajagopalan, R. A novel approach to fabricate macrovoid-free and highly permeable PVDF hollow fiber membranes for membrane distillation. *AIChE J.* **2009**, *55* (3), 828.

(23) Teoh, M. M.; Chung, T. S. Membrane Distillation with Hydrophobic Macrovoid-free PVDF-PTFE Blended Hollow Fiber Membranes *Sep. Purif. Technol.* **2008**, in press.

(24) Khayet, M.; Feng, C. Y.; Kulbe, K. C.; Matsuura, T. Preparation and characterization of polyvinylidene fluoride hollow fiber membranes for ultrafiltation. *Polymer* **2002**, *43*, 3879.

(25) Merkel, G. A.; Murtagh, M. J. Fabrication of low thermal expansion, high porosity cordierite body. U.S. Patent 5,258,150, 1993.

(26) Monticelli, O.; Bottino, A.; Scandale, I.; Capannelli, G.; Russo, S. Preparation amd properties of polysulfone-clay composite membranes. *J. Appl. Polym. Sci.* **2007**, *103*, 3737.

(27) Chung, T. S.; Jiang, L. Y.; Li, Y.; Kulprathipanj, S. Mixed matrix membranes (MMMs) comprising organic polymers with dispersed inorganic fillers for gas separation. *Prog. Polym. Sci.* **2007**, *32*, 483.

(28) Sarti, G. C.; Gostoli, C.; Matulli, S. Low energy desalination processes using hydrophobic membranes. *Desalination* **1985**, *56*, 277.

(29) Phattaranawik, J.; Jiraratananon, R.; Fane, A. G. Heat transport and membrane distillation coefficient in direct contact membrane distillation. *J. Membr. Sci.* **2003**, *212*, 177.

(30) Santoso, Y. E.; Chung, T. S.; Wang, K. Y.; Weber, M. The investigation of irregular inner-skin morphology of hollow fiber membranes at high speed spinning and the solutions to overcome it. *J. Membr. Sci.* **2006**, *282*, 383.

(31) Bonyadi, S.; Chung, T. S.; Krantz, W. B. Investigation of corrugation phenomenon in the inner contour of hollow fibers during the non-solvent induced phase-separation process. *J. Membr. Sci.* **2007**, *299*, 200.

(32) Gryta, M. Long-term performance of membrane distillation process. *J. Membr. Sci.* **2005**, *265*, 153.

(33) Phattaranawik, J.; Jiraratananon, R.; Fane, A. G. Effect of pore size distribution and air flux on mass transport in direct contact membrane distillation. *J. Membr. Sci.* **2003**, *215*, 75.

(34) Jiang, L. Y.; Chung, T. S.; Cao, C.; Huang, Z.; Kulprathipanja, S. Fundamental understanding of nano-sized zeolite distribution in the formation of the mixed matrix single- and dual-layer asymmetric hollow fiber membranes. *J. Membr. Sci.* **2005**, *252*, 89.

(35) Xiao, Y.; Wang, K. Y.; Chung, T. S.; Tan, J. Evolution of nanoparticle distribution during the fabrication of mixed matrix TiO_2-polyimide hollow fiber membranes. *Chem. Eng. Sci.* **2006**, *61*, 6228.

(36) Kast, W.; Hohenthanner, C. R. Mass transfer within the gas-phase of porous media. *Int. J. Heat Mass Transfer* **2000**, *43*, 807.

(37) Kuhn, H.; Fostering, H.-D. *Principles of Physical Chemistry*; Wiley: New York, 2000.

(38) Cussler, E. L. *Diffusion, Mass Transfer in Fluid System*, 2nd ed.; Cambridge University Press: New York, 1997.

(39) Schofield, R. W.; Fane, A. G.; Fell, C. J. D.; Macoun, R. Heat and mass transfer in membrane distillation. *J. Membr. Sci.* **1987**, *33*, 299.

(40) Lawson, K. W.; Lloyd, D. R. Membrane distillation. II. Direct contact MD. *J. Membr. Sci.* **1996**, *120* (1), 123.

(41) Smolders, K.; Franken, A. C. M. Terminology for membrane distillation. *Desalination* **1989**, *72*, 249.

Received for review June 20, 2008
Revised manuscript received February 12, 2009
Accepted March 2, 2009

IE8009704